

A wind model for high energy pulses

J. G. Kirk¹, O. Skjæraasen¹, and Y. A. Gallant²

¹ Max-Planck-Institut für Kernphysik, Postfach 10 39 80, 69029 Heidelberg, Germany

² Service d’Astrophysique, CEA-Saclay, F-91191 Gif-sur-Yvette, France

Abstract. A solution to the σ problem — that of finding a mechanism capable of converting Poynting energy flux to particle-borne energy flux in a pulsar wind — was proposed several years ago by Coroniti and Michel who considered a particular prescription for magnetic reconnection in a striped wind. This prescription was later shown to be ineffective. In this paper, we discuss the basic microphysics of the reconnection process and conclude that a more rapid prescription is permissible. Assuming dissipation to set in at some distance outside the light-cylinder, we compute the resulting radiation signature and find that the synchrotron emission of heated particles appears periodic, in general showing both a pulse and an interpulse. The predicted spacing of these agrees well with observation in the case of the Crab and Vela pulsars. Using parameters appropriate for the Crab pulsar — magnetization parameter at the light cylinder $\sigma_L = 6 \times 10^4$, Lorentz factor $\Gamma = 250$ — reasonable agreement is found with the observed total pulsed luminosity. This suggests that the high-energy pulses from young pulsars originate not in the co-rotating magnetosphere within the light cylinder (as in all other models) but from the radially directed wind well outside it.

Key words: Pulsars: general – pulsars: Crab – MHD – radiation mechanisms: non-thermal

1. Introduction

Recently, the non-axisymmetric “striped pulsar wind” investigated by Coroniti (1990) and Michel (1994) has been reexamined (Kirk & Lyubarsky 2001). A striped wind is a structure similar to a Parker spiral, which is produced by the outward radial advection of magnetic field lines whose foot points are anchored on the surface of the rotating neutron star. However, if the field lines originate from the poles of an obliquely rotating dipole, there exists a region around the equatorial plane where the polarity of the field at a fixed radius reverses at the rotation period of the star, producing stripes of alternating magnetic field direction. Magnetic energy is dissipated into particle energy if reconnection occurs at the stripe boundaries. Coroniti (1990)

proposed that this kind of dissipation proceeds at a rate sufficient to maintain the thickness of the current sheet approximately equal to the gyro radius of the heated particles. Michel (1994) used essentially the same criterion, phrased in terms of the velocity of the current carriers. These early papers concluded that observations of the Crab Nebula, which indicate conversion of Poynting flux to particle-borne energy flux within $10^9 r_L$, (where r_L is the radius of the light cylinder) could be explained by this mechanism. However, Lyubarsky & Kirk (2001) point out that reconnection is accompanied by acceleration of the wind. Both processes occur on the same timescale when the Coroniti/Michel prescription is used for reconnection. This is also the timescale on which the plasma expands. As a result, time dilation in the accelerated flow has to be taken into account and the dissipation rate is significantly reduced — in the case of the Crab, conversion of Poynting flux to particle-borne energy flux is not achieved until roughly $10^{12} r_L$, which is too slow to account for the observations (the so-called σ -problem; see Melatos (1998) and references therein).

In Sect. 2 we discuss the physics of the dissipation process and the prescriptions used to model it. We conclude that it may proceed much more rapidly than suggested by Coroniti and Michel. If rapid reconnection in fact occurs, it will be accompanied by radiation losses (Melatos 1998) that may give rise to an observable signature. In this paper, and in an accompanying letter (Kirk et al. 2002) we adopt this hypothesis. We assume that dissipation is triggered at a surface $r = r_0$ well outside the light cylinder in the supersonic MHD wind of a pulsar and takes place rapidly, so that the plasma does not have time to expand significantly. Using two simple models of the electron distribution we show (i) that for parameters thought typical of the winds from young pulsars (e.g., the Crab) the predicted emission is pulsed, with, in general, a pulse and interpulse that are not symmetrically spaced in phase and (ii) that the predicted synchrotron luminosity in the pulses agrees to order of magnitude with that observed from the high energy emission of the Crab pulsar.

Our calculations suggest that the high energy pulses emitted by young pulsars originate as synchrotron emis-

sion in the pulsar wind, far outside the light cylinder. This is in marked contrast with conventional models of high-energy pulse production at an inner or outer gap — for a review see Harding (2001) — and also with magnetospheric synchrotron based models Machabeli et al (2000), Crusius-Wätzel et al. (2001). The current sheet just beyond the region of closed field lines in the magnetosphere has also been proposed as the source of high energy radiation from the Crab pulsar (Lyubarsky1996). But, in common with the others, this model relies for pulse production on the co-rotation with the star of a beam of radiation emitted from within the light cylinder.

2. Dissipation in the current sheet

An equilibrium solution of the Maxwell-Vlasov equations describing a magnetic reversal across a current sheet was found many years ago (Harris 1962) and was subsequently generalized to apply also to the case of relativistic particle temperatures and drift speeds (Hoh 1968). If, in the special case in which the plasma is composed solely of positrons and electrons the magnetic field strength far from the sheet is B' , the central density of particles of each charge is N' and the sheet width is a , (all measured in the frame of reference in which the sheet is stationary and the electrons and positrons have equal and opposite drift speeds) then the temperature T , which is independent of position in the sheet, is given by

$$T = \frac{B'^2}{16\pi N'} \quad (1)$$

The Debye radius is

$$\lambda_D = \left(\frac{T}{4\pi N' e^2} \right)^{1/2} \quad (2)$$

and is, to within a factor of the order of unity, equal to the gyro radius of a particle of energy T in the magnetic field B' . The speed $\pm c\beta$ with which each component drifts is also independent of position in the sheet and is obtained from

$$\beta = \frac{\lambda_D}{a} \quad (3)$$

The magnetic field reverses across the sheet and the density goes to zero far from the sheet — simple explicit expressions for these quantities as functions of position are available.

This solution is well-known to be unstable to the excitation of a variety of waves — see, for example, Daughton (1999). The standard scenario is that the current sheet first filaments because of the growth of the tearing mode, producing magnetic islands separated by neu-

tral lines. These then lead to magnetic reconnection and its associated dissipation (Melrose 1986). This scenario has largely been developed in the context of the geomagnetic tail of the Earth. Particle-in-cell simulations appear to confirm its validity ([Zhu & Winglee 1996; Pritchett et al. 1996], although the 3-dimensional picture is more complicated (Büchner & Kuska 1999; Hesse et al. 2001).

The key question in the application to pulsar winds is that of how quickly and, therefore, whereabouts in the wind the dissipation occurs. The linear growth rate γ_t of the tearing instability has been calculated in the relativistic case by Zelenyi & Krasnosel'skikh (1979). For $T \gg mc^2$ they find for the most unstable mode, which has a wavelength approximately equal to the sheet thickness,

$$\gamma_t = \beta^{3/2} c/a = \lambda_D^{3/2} c/a^{5/2} \quad (4)$$

The magnetic field far from the sheet and the total number of particles per unit area of sheet ($\approx aN'$) suffice to determine the drift speed. A single additional parameter is then needed to fix the sheet properties. This can be chosen, for example, as the thickness a or the temperature T ; the thinner (cooler) the sheet, the faster the tearing mode grows.

In his model of the high-energy emission from pulsars, Lyubarsky (1996) argues that the rate of dissipation is controlled by the timescale associated with the growth of the tearing mode. Specifically, he assumes that magnetic flux is swept into the sheet and annihilated at a speed given by $a\gamma_t$. This scenario is plausible, although it is not certain that the field dissipation, which presumably occurs at null points created during the field filamentation, proceeds on the timescale of the tearing mode growth. If it operates, it results in strong radiation from the innermost parts of the sheet. The geometry of the flow in this region is, however, uncertain.

Another, simpler, prescription for the speed of dissipation was (implicitly) adopted by both Coroniti (1990) and Michel (1994) and, later, also by Lyubarsky & Kirk (2001). In terms of the magnetic field and the number of particles per unit area in the sheet, the drift speed can be written

$$\beta = \frac{B'}{8\pi a N' e} \quad (5)$$

If the wind expands radially without any dissipation ($a = \text{constant}$), then its speed remains constant so that $B' \propto r^{-1}$ and $N' \propto r^{-2}$. Equation (5) then implies that the drift speed β grows linearly with radius. At a radius where, according to this equation, $\beta > 1$, no equilibrium of the Harris type can exist; the Coroniti/Michel prescription consists in assuming that the sheet thickness grows at a rate just sufficient to avoid this happening. Dissipation

is thus assumed to maintain the current sheet very close to an equilibrium in which $\beta \approx 1$. This enables reconnection to be incorporated straightforwardly into a set of MHD equations describing the pulsar wind. Provided the sheet does not radiate significantly, conservation of energy, momentum and particle number, together with Eq. (3) in which β is set to unity, determine the dynamics of the wind. However, in this case dissipation proceeds on a time scale corresponding to the length r , which is the same scale on which adiabatic expansion of the sheet operates. A careful analysis of the dynamics shows that the wind accelerates and, as a result, the dissipation becomes rather ineffective (Lyubarsky & Kirk 2001).

On the other hand, an instability in the current sheet can communicate itself to the rest of the pulsar wind at the speed of the fast magnetosonic wave, which, for a cold plasma is roughly equal to the Alfvén speed. Recent investigations of reconnection in a relativistic pair plasma (Zenitani & Hoshino 2001) indeed indicate that the relevant timescale is related to the crossing time of a magnetosonic wave. In the case of a transsonic pulsar wind, a magnetosonic wavefront could appear almost stationary in the frame of the observer, so that dissipation could be completed within a few pulsar periods. This is the prescription we adopt in this paper. Energy is assumed to be released in the current sheet at a fixed radius, the position of which is taken as a free parameter. After energy release, we assume the plasma cools slowly as the wind moves radially outwards.

3. Geometry of the emission region

Any radial, relativistic flow containing a periodic modulation of the emissivity is likely to appear pulsed to an observer because of two effects. Firstly, the strong Doppler boosting of approaching parts of the flow means that only a small cone of the flow is visible, propagating within an angle of roughly $1/\Gamma$ with respect to the line of sight, where $\Gamma = (1 - \beta^2)^{-1/2}$ is the Lorentz factor and $c\beta$ the radial speed. The spread in arrival times at the observer of photons emitted at the same radius but at different parts within this cone is roughly $r/(c\Gamma^2)$. Secondly, if emission is restricted to a range Δr in radius, the fact that the photons move only slightly faster than the flow when seen in the laboratory frame means that the spread in arrival times is roughly $\Delta r/(c\Gamma^2)$. For a wind modulated at the period $P = 2\pi r_L/c$ of a rotating star, the approximate condition for the observation of pulsed emission is therefore

$$\Delta r, r \lesssim \Gamma^2 r_L \quad (6)$$

If this is fulfilled, the observed pulse shapes appear similar to the pattern of modulation of the flow. In particular, for a flow containing the corrugated spiral current sheet of an oblique rotator (Fig. 1), there should in general be

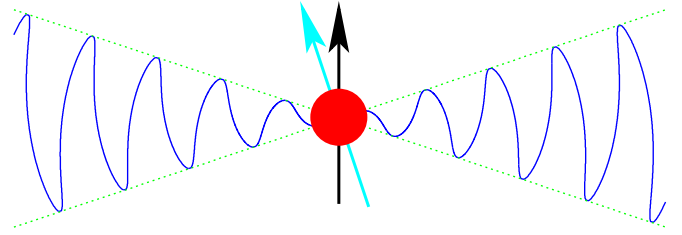


Fig. 1. A meridional section of the current sheet of an oblique rotator with a radial wind. The thin lines limiting the extent of the sheet in latitude depict the plane of the magnetic equator when the magnetic axis lies in the plane of the section.

two components (pulse and interpulse) which are symmetrically placed if the pulsar is viewed from the equatorial plane, but are asymmetrical when viewed from higher latitudes. Denoting by α the angle between the rotation axis and the magnetic axis, and by ζ the angle between the rotation axis and the viewing direction, these pulses appear only for $90^\circ - \alpha < \zeta < 90^\circ + \alpha$.

To improve on the estimate (6) and calculate the expected pulse shapes we adopt the following model of the volume emissivity ϵ of the wind:

- (i) The emission region is located on the current sheet in the super-magnetosonic MHD wind of a rotating neutron star with an oblique, split-monopole magnetic field.
- (ii) The dependence on frequency ν of the volume emissivity is a power-law: $\epsilon \propto \nu^{-a}$.
- (iii) The emission switches on abruptly as plasma in the sheet crosses the surface $r = r_0$. Thereafter the volume emissivity decays as a power law in radius: $\epsilon \propto r^{-2-q}$.

Outside the light cylinder, assumption (i) should be a good approximation, independent of the actual configuration of the magnetic field close to the pulsar surface. The assumption that emission occurs only at the exact position of the current sheet is an idealization — in reality, the entire flow may be modulated, making the observed pulse more complex. In this case, our computations provide the Greens function with which the pattern is to be folded to find the observed pulse shape. In the ultra-relativistic limit, a simple wind solution is available (Bogovalov 1999) in which the velocity is radial and constant and the magnetic field is almost toroidal. The thin current sheet in such a wind is described by the equation

$$\begin{aligned} r &= r_s(\theta, \phi, t) \\ &= \beta r_L [\pm \arccos(-\cot \alpha \cot \theta) + ct/r_L - \phi + 2n\pi] \end{aligned} \quad (7)$$

(Kirk & Lyubarsky 2001), where (r, θ, ϕ) are polar coordinates, t is the observer-frame time and n is an integer.

Assumption (ii) is an idealization that ensures the pulse shape is independent of frequency. In reality, the electron distribution may exhibit breaks and cut-offs, which will be translated into different pulse shapes at different frequencies. Our assumption, however, ensures that all parts of the flow can contribute to the emission at a given frequency, making it harder to obtain sharply defined pulses.

The dependence of the observed flux F on t , α and the direction of observation $\hat{\mathbf{n}}$ is:

$$F \propto \int_{-\infty}^{+\infty} dt' \int_{r_0}^{\infty} dr \int_{90^\circ-\alpha}^{90^\circ+\alpha} d\theta \int_0^{2\pi} d\phi r^{-q} D^{2+a} \delta[r - r_s(\theta, \phi, t')] \delta(t' - t + \hat{\mathbf{n}} \cdot \mathbf{r}/c) \quad (8)$$

where $D = 1/(1 - \beta \hat{\mathbf{r}} \cdot \hat{\mathbf{n}})$ is the conventionally defined Doppler factor, apart from a (constant) factor of Γ . Choosing $a = 0$ and $q = 3$, which is appropriate for the synchrotron radiation of a fixed number of particles that undergo predominantly adiabatic losses in the expanding plasma, we present sample pulses for various Lorentz factors in Fig. 2. For the higher Lorentz factors this figure also displays the effect of a faster fall-off of the emissivity towards higher radii ($q = 6$), mimicking the effect of an accelerating wind. The asymmetry in time of the pulses is produced by our assumption of a sudden switching on of the emission and is reduced by a more rapid switching off. The parameters of this figure have been chosen to correspond to the Crab Pulsar. The radio emission of this object is complex, but is known to display ‘core emission’ in the radio precursor (Rankin (1990), which strongly suggests that the magnetic axis passes within a few degrees of the line of sight. This indicates that the inclination angle α of the magnetic axis to the rotation axis roughly equals the angle ζ between the rotation axis and the line of sight. The latter is determined by X-ray and optical observations of the ‘torus’ (Aschenbach & Brinkmann 1975; Hester et al. 1995) to be 60° . In Fig. 2 the emission has been assumed to switch-on at $r_0 = 30r_L$ and pulses appear for $\Gamma > 5$, in rough agreement with the estimate (6). At higher Lorentz factors, the pulses sharpen. From Eq. (7) it can be seen that the emission splits naturally into two contributions, corresponding to different signs of the term $\arccos(-\cot \alpha \cot \theta)$. In the first two plots of Fig. 2 these contributions are plotted separately as dotted lines. Although the detailed pulse shapes will depend on the structure of the reconnecting sheets in the Crab wind, as well as the details of the switching on mechanism and the amount of acceleration of the wind, the separation of the two peaks is not sensitive to these unknowns, being determined by the location of the sheets. This separation in phase equals $\arccos(\cot \alpha \cot \zeta)/180^\circ$, corresponding to 0.39 for the Crab Pulsar, in good agreement with observation (e.g., Kanbach (1998)).

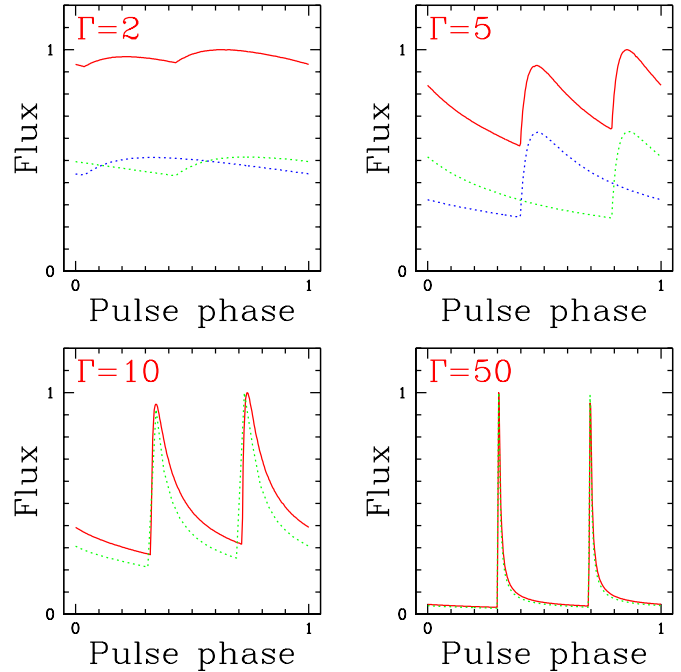


Fig. 2. Pulse shapes obtained by a numerical integration of Eq. (8). Four values of the Lorentz factor (Γ) are shown, the remaining parameters are: $\alpha = 60^\circ$, $\zeta = 60^\circ$, $r_0 = 30r_L$, $a = 0$ and $q = 3$ (see text). The total emission is shown as a solid line. For $\Gamma = 2$ and 4, the contributions of the current sheets of different polarity are shown as dotted lines. For $\Gamma = 10$ and 50, the dotted line shows the effect of a more rapid fading of the emissivity to larger radius ($q = 6$).

In the case of the Vela pulsar, conflicting interpretations of the polarization sweep and the X-ray morphology have yielded $\alpha \approx 71^\circ$, $\zeta \approx 65^\circ$ in one case (Radhakrishnan & Deshpande 2001) and $\alpha \approx \zeta = 53^\circ$ in the other (Helfand et al. 2001). These imply separations of the gamma-ray (sub-)pulses of 0.45 and 0.31 of a period respectively, so that the observed spacing of 0.4 marginally favors the former interpretation.

4. Luminosity estimates

Electrons heated in the current sheets will enter the surrounding magnetic field and emit synchrotron radiation. A rough estimate of the power radiated can be found by assuming a monoenergetic electron population of Lorentz factor $\gamma (\gg 1)$ and requiring pressure equilibrium between the hot plasma and the surrounding magnetic field. Taking the single particle synchrotron emissivity to be a delta function in frequency, the luminosity at frequency ν into a solid angle Ω is given by

$$\frac{dL}{d\nu d\Omega} \approx \int_{r_0}^{\infty} dr r^2 \Delta \Gamma n'_h P_{s.p.} \delta(\nu - \nu_0) \quad (9)$$

(Skjæraasen & Kirk 2001), where Δ (≤ 1) is the fraction of a wavelength of the wind pattern occupied by hot electrons of proper density n'_h , $P_{s.p.} = (4/3)c\sigma_T\gamma^2(B'^2/8\pi)$ is the synchrotron power emitted by a single electron, and ν_0 is the characteristic frequency of emission, measured in the observer frame (σ_T is the Thomson cross section). The condition of pressure equilibrium gives $n'_h\gamma mc^2/3 = B'^2/8\pi$, where B' is the magnetic field in the co-moving frame and m the electron mass. Well outside the light cylinder, but before energy release begins; i.e., at $r_L < r < r_0$, the density and magnetic field scale as r^{-2} and r^{-1} respectively, and can be characterized by the values n_L and B_L obtained by extrapolating back to $r = r_L$. Provided the flow does not accelerate significantly whilst emitting synchrotron radiation, these same scalings, which imply γ independent of r , can be used in the integration in Eq. (9). This is convenient for a rough estimate of the luminosity, but is sensitive to the assumption that the wind does not accelerate upon reconnection.

If we identify the ratio of Poynting flux to kinetic energy (at the light cylinder) $\sigma_L = B_L^2/(4\pi\Gamma n_L mc^2)$, define an average fraction of hot particles $\bar{\Delta} = r_0 \int_{r_0}^{\infty} dr \Delta/r^2 \lesssim 1$, and use the standard relation $B_L = 2.9 \times 10^8 \dot{P}^{1/2} P^{-5/2}$ G, the luminosity becomes

$$\frac{d\hat{L}}{d\Omega} = 3.9 \times 10^7 \left(\frac{\sigma \bar{\Delta} r_L \dot{P}}{\Gamma^3 r_0 P^4} \right) \quad (P \text{ in secs}) \quad (10)$$

where $d\hat{L}/d\Omega$ is the synchrotron luminosity per steradian divided by the total wind luminosity per steradian. Similarly, the characteristic frequency is

$$h\nu_0(r) = 2.6 \times 10^{-6} \left(\frac{r_L}{r} \right) \sigma^2 \dot{P}^{1/2} P^{-5/2} \text{ (MeV)}. \quad (11)$$

The spectrum produced by this simple model with monoenergetic electrons extends to a maximum frequency given by Eq. (11) with $r = r_0$ and is flat: $dL/d\nu d\Omega \propto \nu^0$. However, this aspect is sensitive to the way in which the plasma expands and accelerates after reconnection. If, in a more realistic scenario, the electron density is a power law $N(\gamma) \propto \gamma^{-p}$, with $p > 2$, then most of the energy resides in the particles with lowest γ and the above estimate (11) refers to the photons emitted by these particles. The emission at frequencies $\nu < \nu_0(r_0)$ is dominated by the same low energy particles radiating at larger radius in a weaker magnetic field, and is determined by the expansion and acceleration of the hot plasma. In the absence of acceleration, the flat spectrum derived above prevails. However, the intrinsic spectrum, which is a power law $dL/d\nu d\Omega \propto \nu^{-a}$, with $a > 0.5$, is revealed at frequencies $\nu > \nu_0(r_0)$, where particles radiating at r_0 dominate. In the case of the Crab pulsar, the optical to X-ray emission is consistent with a flat spectrum (Shearer & Golden 2001), which steepens to $a > 1$ at a photon energy of approximately 1 MeV (Kanbach 1998; Kuiper et al. 2001). Equation (11) therefore implies $\sigma = 1.1 \times 10^4 \sqrt{r_0/r_L}$. Observations suggest $d\hat{L}/d\Omega \approx 10^{-3}$ for this object, which,

from Eq. (10), is consistent with a mildly supersonic flow, $\Gamma \approx 250$, that starts to radiate at $r_0 = 30r_L$. This is consistent with the lower limit of $5r_L$ found by (Bogovalov & Aharonian 2000) for the radius at which the conversion of Poynting flux to particle-born flux may occur.

5. Discussion

Current models of the high energy emission from rotation powered pulsars fall loosely into two groups: “polar cap” and “outer gap” models (for a recent review see Harding (2001)). Each of these places the emission region in the corotating magnetosphere of the star. The predicted pulse shapes depend sensitively on the uncertain geometry of the magnetic field in this region, which is usually assumed dipolar. In contrast, in the model presented above, pulses are emitted well outside the co-rotation region. Provided the pulsar drives a supersonic, MHD wind, the field geometry approaches a simple asymptotic solution (Bogovalov 1999), which determines the basic properties of the pulses.

In a series of papers, Pacini (1971), Pacini & Salvati (1983), Pacini & Salvati (1987) suggested that particles close to the light cylinder emit synchrotron radiation and are responsible for the optical pulses of the Crab and other pulsars — a theory which appears to be in reasonable agreement with observation (Shearer & Golden 2001). The model presented here is similar in that the radiation mechanism is synchrotron emission and the scaling of Eq. (10) is close to that originally given by Pacini (1971). It goes further, however, by specifying for the emission region a precise geometrical structure and location.

It is known that the dilution of the plasma in the wind must lead to non-ideal MHD behavior (Usov 1975, Michel 1982) and so can be responsible for triggering the emission. The position at which this occurs depends on the initial concentration of charges in the current sheet and is taken as a free parameter. The major uncertainty in the model is the speed with which dissipation proceeds. Our computations implicitly assume rapid dissipation (over a scale small compared to the radius). In this case, it is possible to make a rough estimate of the synchrotron luminosity which is in agreement with observations. A more detailed comparison with the wealth of relevant observations of optical, X-ray and gamma-ray pulsars must await further modeling. It is also conceivable that at least part of the radio emission could be produced in the wind region, as is suggested by the similarity of the pulse profiles at all frequencies seen in the Crab pulsar. However, until a candidate coherent mechanism can be identified, this connection remains very speculative. Nevertheless, the wind scenario is a viable alternative to current theories of gamma-ray, X-ray and optical pulses from rotation-driven pulsars and has the advantage of making specific predictions of the pulse properties.

Acknowledgements. This work is a collaboration of the TMR Network “Astroplasmaphysics” of the European Commission, contract FMRX-CT-98-0168. Y.G. is supported by a Marie Curie Fellowship from the European Community, contract no. HPMFCT-2000-00671 under the IHP programme. J.K. thanks the Wilhelm and Else Heraeus-Stiftung and the conference organisers for their invitation to attend and their hospitality at the meeting, and thanks the other participants for stimulating discussions.

References

- Arons J. 1996 *Space Science Reviews*, 75, 235
 Aschenbach B., Brinkmann W. 1975 *A&A* 41, 147
 Bogovalov S.V., 1999 *A&A* 349, 1017
 Bogovalov S.V., Aharonian F.A. 2000 *MNRAS* 313, 504
 Büchner J., Kuska J.P. 1999 *Ann. Geophys.* 17, 604
 Coroniti F.V. 1990 *ApJ* 349, 538
 Crusius-Wätzel A.R., Kunzl T., Lesch H. 2001 *ApJ* 546, 401
 Daughton W. 1999 *Phys. Plasmas* 6, 1329
 Harding A.K. 2001 in ‘High energy gamma-ray astronomy’ eds: F. Aharonian, H.J. Völk, AIP.
 Harris E.G. 1962 *Nuovo Cimento* 23, 115
 Helfand D.J., Gotthelf E.V., Halpern J.P. 2001 *ApJ* 556, 380
 Hesse M., Kuznetsova M., Birn J. 2001 *J. Geophys. Res. Space Phys.* 106, 29831
 Hester J.J. et al. 1995 *ApJ* 448, 240
 Hoh F.C. 1968 *Physics Fluids* 9, 277
 Kanbach G., 1998 *Adv. Space Res.* 21, 227
 Kirk J.G., Lyubarsky Y. 2001 *Publ. Astron. Soc. Aust.* 18, 415
 Kirk J.G., Skjæraasen O., Gallant Y.A. 2002 *A&A letters*, submitted.
 Kuiper L., Hermsen W., Cusumano G., Diehl R., Schönfelder V., Strong A., Bennett K., McConnell M.L. 2001 to appear in *A&A* (astro-ph/0109200)
 Lyubarsky Y. 1996 *A&A* 311, 172
 Lyubarsky Y., Kirk J.G. 2001 *ApJ* 547, 437
 Machabeli G.Z., Luo Q., Melrose D.B., Vladimirov S. 2000 *MNRAS* 312, 51
 Melatos A. 1998 *Mem. Soc. Ast. It.*, 69, 1009
 Melrose D.B. 1986 “Instabilities in space and laboratory lasers”, Cambridge University Press, Cambridge
 Michel, F.C., 1982 *Rev. Mod. Phys.* 54, 1
 Michel, F.C., 1994 *ApJ* 431, 397
 Pacini F. 1971 *ApJ* 163, L17
 Pacini F., Salvati M. 1983 *ApJ* 274, 369
 Pacini F., Salvati M. 1987 *ApJ* 321, 447
 Pritchett P.L., Coroniti F.V., Decyk V.K. 1996 *J. Geophys. Res. Space Phys.* 101, 27413
 Radhakrishnan V., Deshpande A.A. 2001 *A&A* 379, 551
 Rankin J.M. 1990 *ApJ* 352, 247
 Skjæraasen O., Kirk J.G. 2001 in “Similarities and universality in relativistic flows” Eds: Georganopoulos, Guthmann, Manolakou, Marcowith (Logos Verlag, Berlin)
 Shearer A., Golden A. 2001 *ApJ* 547, 967
 Usov V.V., 1975 *Astrophys. & Space Sci.* 32, 375
 Zelenyi L.M., Krasnosel’skikh V.V. 1979 *Sov. Phys. A.J.* 56, 819
 Zenitani S., Hoshino M. 2001 *ApJ* 562, L63
 Zhu Z.W., Winglee R.M. 1996 *J. Geophys. Res. Space Phys.* 101, 4885